Multistability in mesoscopic Rydberg-atom systems

F. Casagrande and L. A. Lugiato
Dipartimento di Fisica dell'Università, Via Celoria 16, I-20133 Milano, Italy

W. Lange and H. Walther
Max-Planck-Institut für Quantenoptik, D-85748 Garching bei München, Germany
(Received 30 November 1992)

We describe a system of N two-level Rydberg atoms which travel through a resonant cavity and interact with a single mode of the resonator. N is assumed to be on the order of a few tens or hundreds of atoms. In particular, we analyze the case where the atoms are injected in the lower state (absorber) and the system is driven by an external coherent radiation field resonant with the atoms and the cavity. While the analogous system in the optical domain displays standard bistability, the results we obtain for monoenergetic Rydberg atoms are substantially different. The switching behavior is not governed by saturation, but by the Rabi cycles of the atoms in the cavity. The hysteresis cycle of the population of the upper level is butterfly shaped. When the bistability parameter exceeds an appropriate second threshold, the system displays multistability rather than simple bistability, and under proper conditions it develops domains of instability in positive-slope regions of the steady-state curve. We analyze the effects of a velocity distribution (thermal or Gaussian) of the atomic beam, and of inhomogeneous broadening caused by stray electric fields. Finally, we discuss the feasibility of an experimental observation of the effects predicted by our analysis.

PACS number(s): 42.52.+x, 42.65.Pc

I. INTRODUCTION

The interaction of a single cavity mode and a system of two-level atoms is a central problem in modern optics. Its investigation has led to the understanding of several fundamental phenomena such as the Jaynes-Cummings oscillations [1], maser and laser action [2], superradiance and superfluorescence [3], as well as optical bistability [4]. In a macroscopic system, with a large number $N \gg 1$ of atoms in the cavity, these effects are adequately described in terms of semiclassical equations, neglecting quantum fluctuations.

Recent developments in cavity quantum electrodynamics [5] have led to the investigation of the microscopic regime ($N < 1$), in which even the interaction with a single atom can change the state of the radiation field significantly. Experimental realizations of such a system are based on the strong coupling between a single atom and the cavity mode, either using Rydberg atoms in a superconducting high-Q rf resonator, as in the micromaser [6–8], or atoms in an optical microcavity with a large finesse [9]. Under such conditions, the behavior of the system is strongly affected, and often dominated by quantum fluctuations. In the case of microwave systems, thermal fluctuations are also significant. Therefore, a quantum treatment of the electromagnetic field is necessary.

In this paper we consider a new regime for nonlinear optical systems, intermediate between that considered in macroscopic theories ($N \gg 1$) and that typical of microscopic systems ($N < 1$). We assume the number of atoms N to be on the order of 10 to 100, and values of the saturation photon number such that, in first approximation, the semiclassical description is still valid. We will call this intermediate regime *mesoscopic*. It corresponds to the border region, in which the semiclassical picture ceases to be meaningful, and the macroscopic and microscopic descriptions merge into each other.

In the optical domain, an experimental and theoretical investigation of a mesoscopic regime was carried out by Kimble and collaborators [9]. In this paper we analyze the case of Rydberg-atom systems, obtaining substantially different results. As in the micromaser, a beam of two-level Rydberg atoms is injected into a superconducting microwave cavity close to resonance with the atomic transition. The state of the field inside the resonator is inferred from the count rate of atoms in the upper or lower level, after they have left the cavity.

An important property of such a system is that the spontaneous-emission lifetime is very long with respect to all other characteristic times. Consequently, transit broadening is the main mechanism determining the atomic linewidth, instead of providing only a small correction as in the optical regime. In the semiclassical description, based on Maxwell-Bloch equations, transit broadening cannot be adequately described by means of phenomenological atomic damping terms. For this reason, we describe explicitly the atomic motion during the time of flight of the atoms in the cavity.

The problem of the free-running Rydberg-atom maser, under conditions similar to those defined above, has been considered elsewhere [10]. In this paper we will focus, instead, on the case of systems driven by an external coherent field injected into the cavity. If the two-level atoms

enter the cavity in the excited state, one has an amplifier with injected signal or a maser with injected signal, according to whether in the limit of vanishing driving field one recovers a free running maser below or above threshold. If, instead, the two-level atoms enter the cavity in the lower state, the atoms do not amplify but absorb the radiation, and one has a situation analogous to that of standard optical bistability [4]. We have mainly investigated the absorber case and, for the sake of simplicity, limited our analysis to the case in which the input field, the atoms, and the cavity mode are exactly on resonance. This corresponds to the situation which in the standard theory is called *purely absorptive bistability* [4].

First we consider the case of a monoenergetic atomic beam. The fact that the atomic linewidth is determined by transit broadening leads to substantial changes in the behavior of the system with respect to the standard picture of absorptive optical bistability.

(1) The mechanism of switching between the branches of the bistable hysteresis cycle is not based on the saturation of absorption, but on the Rabi cycles undergone by the atoms in the cavity. As a consequence, the hysteresis cycle of the intracavity field amplitude as a function of the input field amplitude exhibits points of transparency (bleaching) whenever the atoms perform an exact number of Rabi cycles during their flight through the cavity. The difference from the case of optical bistability becomes apparent especially in the hysteresis cycle of the population of the upper level, which in the case of Rydberg atoms is butterfly shaped, in contrast to the usual ring shape.

(2) When the value of the bistability parameter exceeds a suitable second threshold, the system exhibits multistability rather than simple bistable behavior. In the case of standard optical bistability, multistable behavior can arise only when the system operates with more than one cavity mode and out of resonance.

(3) When the product $k\tau$ of the cavity damping rate k and the flight time τ of the atoms in the cavity is on the order of unity or larger, the system develops instabilities in parts of the positive-slope branches of the steady-state curve. These instabilities can produce spontaneous undamped oscillations in the output intensity, which will be analyzed in a subsequent paper [15]. In the case of standard optical bistability in the single-mode regime, spontaneous oscillations can appear only under off-resonance conditions.

Next, we extend our analysis of the steady-state behavior to the case where the atomic beam displays a velocity distribution, which is assumed to be either thermal or Gaussian. In the former case, the behavior of the system resembles that of standard optical bistability; for example, no multistability is found at resonance. We also analyze the effects of inhomogeneous broadening caused by stray electric fields in the cavity. Finally we discuss the feasibility of observing the effects predicted by our theory using an experimental setting realized at the Max-Planck-Institut für Quantenoptik.

In Sec. II we describe our model. Sections III and IV are devoted to the description of the steady-state behavior in the monoenergetic case and to the linear stability analysis of the stationary solutions, respectively. In Sec. V we study the effects of a velocity distribution and of inhomogeneous broadening. In Sec. VI we discuss the feasibility of experimental observation of the predicted phenomena, while Sec. VII provides a survey of our results.

II. THE MODEL

We start by discussing a basic model with a monoenergetic atomic beam and homogeneous time-of-flight broadening of the atomic line. We assume that, after an initial transient, one cavity mode, uniform in the longitudinal direction, is excited, and the coupling of atoms to all other modes is completely negligible. Under these assumptions, the dynamics of the system can be described by the following Maxwell-Bloch equations in the slowly varying envelope approximation:

$$\frac{d\alpha_0(t)}{dt} = -k[(1+i\theta)\alpha_0(t) - \alpha_{\rm in}] + \frac{g}{L}\int_0^L dz\, R^-(z,t), \tag{2.1a}$$

$$\left(\frac{\partial}{\partial t} + v_0\frac{\partial}{\partial z}\right) R^-(z,t) = 2g\alpha_0(t)\, R_3(z,t) - i\delta\, R^-(z,t), \tag{2.1b}$$

$$\left(\frac{\partial}{\partial t} + v_0\frac{\partial}{\partial z}\right) R_3(z,t) = -g[\alpha_0(t)\, R^+(z,t) + \alpha_0^*(t)\, R^-(z,t)], \tag{2.1c}$$

plus the complex conjugates of Eqs. (2.1a) and (2.1b). In Eqs. (2.1) the two-level Rydberg atoms are described by the position-dependent macroscopic polarization $R^{\pm}$ and (one-half) the population inversion R_3. The quantity α_0 is the complex amplitude of the cavity mode ($|\alpha_0|^2 = n$ being the mean photon number in the cavity). The system parameters are the cavity linewidth k, defined in terms of the cavity frequency ω_c and the quality factor Q of the cavity

$$k = \frac{\omega_c}{2Q}, \tag{2.2}$$

the Jaynes-Cummings coupling constant [1] g ($2g$ being the *one-photon Rabi frequency*), the atomic detuning δ

$$\delta = \omega_a - \omega_{\rm in}, \tag{2.3}$$

where ω_a is the atomic transition frequency and $\omega_{\rm in}$ is the frequency of the incident field, the normalized cavity detuning θ

$$\theta = \frac{\omega_c - \omega_{\rm in}}{k}, \tag{2.4}$$

the cavity length L, and the amplitude $\alpha_{\rm in}$ of the coherent driving field ($k|\alpha_{\rm in}|^2$ being the photon flux entering the cavity).

In the field equation (2.1a), the atomic polarization distributed in the cavity acts as a source for the oscilla-

tion of the cavity mode, together with the injected signal. Equations (2.1b) and (2.1c) are the optical Bloch equations, with atoms moving at velocity v_0 in the z direction. The convective derivative on the left-hand side (lhs) takes into account changes of the Bloch vector in time as well as due to the propagation of atoms.

In the optical domain, where radiative decay is the main source of atomic damping, there are additional phenomenological damping terms in the Bloch equations. For Rydberg transitions, however, radiative damping is negligible. This is why damping terms are absent in our atomic equations. Instead, in the limit of negligible inhomogeneous effects, the atomic linewidth is mainly determined by transit broadening. It is included in the Maxwell-Bloch equations (2.1b) and (2.1c) via the propagation of the atoms along the cavity. It must be stressed that this is a peculiar feature of systems operating with Rydberg transitions. For atomic beams whose transitions are in the optical domain, transit broadening is only a small correction to radiative broadening [9].

The familiar description of atomic dynamics in terms of the evolution of the Bloch vector will prove very useful throughout our analysis. From equations (2.1b) and (2.1c), the conservation of the modulus of the Bloch vector is easily checked

$$\left(\frac{\partial}{\partial t}+v_0\frac{\partial}{\partial z}\right)\left[R^+(z,t)R^-(z,t)+R_3^2(z,t)\right] \equiv \left(\frac{\partial}{\partial t}+v_0\frac{\partial}{\partial z}\right)\frac{N^2(z,t)}{4}=0. \quad (2.5)$$

Assuming that the number of atoms per unit length $N(z,t)/L$ is stationary, (2.5) implies that $N(z,t)=N$ is a constant, equal to the total number of atoms in the cavity. We can use this result to introduce one-atom variables $r^{\pm}(z,t)$ and $r_3(z,t)$ defined by

$$R^{\pm}(z,t)=N\,r^{\pm}(z,t), \quad R_3(z,t)=N\,r_3(z,t), \quad (2.6)$$

with $r^+r^-+r_3^2=1/4$.

We can also parametrize the atoms by their time of flight τ in the cavity rather than their position introducing a new variable

$$z'\equiv\frac{z}{v_0}, \quad 0\le z'\le\frac{L}{v_0}\equiv\tau. \quad (2.7)$$

Using Eqs. (2.6) and (2.7), the Maxwell-Bloch equations (2.1) assume the following form:

$$\frac{d\alpha_0(t)}{dt}=-k[(1+i\theta)\alpha_0(t)-\alpha_{\rm in}]+\frac{gN}{\tau}\int_0^\tau dz'\,r^-(z',t), \quad (2.8a)$$

$$\left(\frac{\partial}{\partial t}+\frac{\partial}{\partial z'}\right)r^-(z',t)=2g\alpha_0(t)\,r_3(z',t)-i\delta\,r^-(z',t), \quad (2.8b)$$

$$\left(\frac{\partial}{\partial t}+\frac{\partial}{\partial z'}\right)r_3(z',t)=-g[\alpha_0(t)\,r^+(z',t)+\alpha_0^*(t)\,r^-(z',t)]. \quad (2.8c)$$

We consider atoms injected into the cavity at $z'=0$ with zero polarization $[r^{\pm}(0,t)=0]$, either in the upper state $[r_3(0,t)=1/2]$ or in the lower state $[r_3(0,t)=-1/2]$. In the former case our model equations (2.8) describe the dynamics of a maser (or amplifier) with injected signal; in the latter case, they describe the dynamics of an absorber. In most of our discussion we will focus on the absorber.

III. STEADY-STATE ANALYSIS

A. Steady-state equation

In this section we discuss the steady-state behavior of the system. With α_0, $r^{\pm}$, and r_3 independent of time, Eqs. (2.8) reduce to

$$0=\alpha_{\rm in}-(1+i\theta)\alpha_0+\frac{gN}{k\tau}\int_0^\tau dz'\,r^-(z'), \quad (3.1a)$$

$$\frac{d}{dz'}r^-(z')=2g\alpha_0\,r_3(z')-i\delta\,r^-(z'), \quad (3.1b)$$

$$\frac{d}{dz'}r_3(z')=-g\left[\alpha_0\,r^+(z')+\alpha_0^*\,r^-(z')\right], \quad (3.1c)$$

plus the complex conjugates of Eqs. (3.1a) and (3.1b). The initial conditions are

$$r^{\pm}(0)=0, \qquad r_3(0)=\pm\frac{1}{2}, \quad (3.2)$$

where the upper (lower) sign indicates the amplifier (absorber). From the atomic equations (3.1b) and (3.1c) we easily obtain

$$r^-_{\downarrow\uparrow}(z')=\pm\frac{g\alpha_0}{\Omega}\left\{\sin(\Omega z')-i\frac{\delta}{\Omega}\left[1-\cos(\Omega z')\right]\right\}, \quad (3.3a)$$

$$r_{3\downarrow\uparrow}(z')=\pm\frac{1}{2}\mp\frac{4g^2|\alpha_0|^2}{\Omega^2}\sin^2\left(\frac{\Omega z'}{2}\right)=\pm\frac{1}{2}\mp P_{\downarrow\uparrow}(z'), \quad (3.3b)$$

where on the lhs the arrow pointing downwards (upwards) means a quantity calculated starting from $r_3(0)=1/2$ $(-1/2)$; upper and lower signs must be taken concurrently in Eqs. (3.3). The generalized Rabi frequency Ω is defined as

$$\Omega=\sqrt{4g^2|\alpha_0|^2+\delta^2}\equiv\sqrt{\Omega_0^2+\delta^2}. \quad (3.4)$$

In Eq. (3.3b) $P_\downarrow$ ($P_\uparrow$) is the probability for occupation of the lower (upper) state.

Inserting the result (3.3a) for the atomic polarization, Eq. (3.1a) provides a closed steady-state equation for the cavity field amplitude α_0. Introducing dimensionless cavity (x) and input (y) field amplitudes

$$x=2g\alpha_0\tau, \qquad y=2g\alpha_{\rm in}\tau, \quad (3.5)$$

and a cooperation parameter C, proportional to the ratio of gain to losses

$$C=\frac{Ng^2\tau}{4k}, \quad (3.6)$$

the steady-state equation reads

$$y = x\left[1 \mp 4C\frac{1-\cos\sqrt{|x|^2+(\delta\tau)^2}}{|x|^2+(\delta\tau)^2} + i\left(\theta \pm 4C\delta\tau\frac{1-\operatorname{sinc}\sqrt{|x|^2+(\delta\tau)^2}}{|x|^2+(\delta\tau)^2}\right)\right], \quad (3.7)$$

where the upper (lower) sign must be selected in the case of an amplifier (absorber) and the function $\operatorname{sinc}(x) \equiv \sin(x)/x$ is used. In order to gain physical insight and because of its importance, in our subsequent analysis, we concentrate on the resonant case [$\delta = \theta = 0$ in Eq. (3.7)]. In this situation, assuming for definiteness that the input field y is real, the steady-state intracavity field x is also real and Eq. (3.7) becomes

$$y = x \mp 4C\frac{1-\cos x}{x}. \quad (3.8)$$

Note that in the case of atoms injected in the excited state and in the absence of an external field, Eq. (3.8) reduces to $x^2 = 4C(1-\cos x)$ or ${\alpha_0}^2 = (N/2k\tau)\sin^2(g\alpha_0\tau)$, which is the micromaser stationary equation for the mean photon number in the semiclassical limit, neglecting quantum and thermal fluctuations [11]. The first micromaser threshold, obtained in the limit $x = 0$, corresponds to $C = 1/2$, which is the same threshold value as for a resonant, homogeneously broadened standard laser with the cooperation parameter (here called $C_{\rm opt}$) defined as [4]

$$C_{\rm opt} = \frac{Ng^2}{2k\gamma_\perp}, \quad (3.9)$$

$\gamma_\perp$ being the atomic linewidth. This coincidence is one of the reasons for choosing the definition (3.6) of the cooperation parameter. The comparison of Eqs. (3.6) and (3.9) illustrates that radiative decay is replaced by the finite transit time as the mechanism of line broadening for Rydberg transitions, as opposed to optical transitions.

B. Nonlinear absorber

We start by discussing the case of the absorber, described at steady state by the equation

$$y = x + 4C\frac{1-\cos x}{x}. \quad (3.10)$$

First of all, Eq. (3.10) can be compared with the corresponding equation in the optical domain, the well-known state equation of absorptive optical bistability [4]

$$y = x + 2C_{\rm opt}\frac{x}{1+x^2}, \quad (3.11)$$

where $C_{\rm opt}$ is defined in Eq. (3.9). We see that the nonlinearity is completely different in the two cases. Actually, Eqs. (3.10) and (3.11) describe similar behavior only in the two opposite linear regimes, either at very low incident field amplitudes $y \ll 1$, where

$$x \simeq \frac{y}{1+2C}, \quad (3.12)$$

or at very high field $y \gg 1$, $y \gg C$, where

$$x \simeq y. \quad (3.13)$$

Hence Eq. (3.10) implies a cooperative linear regime at low incident power, and an asymptotic linear regime at high incident power, comparable with the saturated regime in the optical domain. In general, the cubic state equation (3.11) implies bistability for $C_{\rm opt} > 4$ [4]; in contrast to that, the presence of an *oscillating nonlinearity* in Eq. (3.10) suggests the possibility of *multistable behavior* for Rydberg atoms.

Figure 1 shows the steady-state diagrams obtained from Eq. (3.10) for different values of the cooperation parameter C. If we tentatively attribute a stable (unstable) nature to all sections of the $x(y)$ curve with positive (negative) slope (the precise discussion of the stability will be given in Sec. IV), we find examples of monostability ($C = 0.5$), bistability ($C = 2$), and tristability ($C = 4$). The bistability and tristability thresholds are at $C = 0.85$ and $C = 2.47$, respectively. In general, the curve $y(x)$ defined in Eq. (3.10) has inflection points $\bar{x}$ which obey the equation

$$1 + \left(\frac{\bar{x}^2}{2} - 1\right)\cos\bar{x} = \bar{x}\sin\bar{x}. \quad (3.14)$$

The threshold values of C for the appearance of parts with negative slope (i.e., the appearance of new hysteresis loops) correspond to the cases where one of these inflection points has a horizontal tangent $[(dy/dx)_{\bar{x}} = 0]$. Using this condition together with Eq. (3.14) one obtains that the threshold values of the parameter C are the positive values of

$$C_{\rm thr} = -\frac{1}{2\cos\bar{x}}. \quad (3.15)$$

The values of $C_{\rm thr}$, $\bar{x}$ and $\bar{y} = y(\bar{x})$ thus calculated are reported in Table I for the first four hysteresis loops.

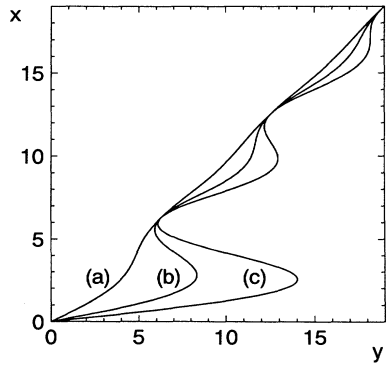

FIG. 1. Multistability in the nonlinear absorption with a beam of two-level Rydberg atoms: dimensionless cavity field amplitude x vs incident field amplitude y from the resonant steady-state equation (3.10). (a) Cooperation parameter $C = 0.5$; (b) $C = 2$; (c) $C = 4$.

TABLE I. Threshold values for the occurrence of the first four hysteresis loops, calculated from Eq. (3.10) for the resonant stationary absorber. At the points $(\bar{x}, \bar{y})$ the function $y(x)$ defined by Eq. (3.10) has an inflection.

Loops	C_{thr}	$\bar{x}$	$\bar{y}$
1	0.85242	4.08557	5.40966
2	2.47354	10.79203	11.89416
3	4.05426	17.15512	18.21702
4	5.62938	23.47301	24.51751

Hence, in the case of Rydberg atoms, multistability (or more precisely the coexistence of more than two stable stationary states) is possible even in the regime of single-mode operation, whereas in the optical domain multistability requires the involvement of two or more longitudinal modes of the cavity [4]. This difference can be understood by considering in detail the mechanism which produces bi- or multistability in the case of Rydberg atoms. As a matter of fact, we note in Fig. 1, as well as directly from Eq. (3.10), the presence of *bleached states* defined by the condition

$$x_m = y_m = 2m\pi \quad (m = 1, 2, \ldots), \tag{3.16}$$

for which the outgoing x reduces to the value of the incident field y. In these states, the atomic Bloch vector performs an integer number of rotations during the passage through the cavity, because $\Omega_{0,m} = m(2\pi/\tau)$. Each rotation corresponds to a cycle of absorption and emission of radiation exchanged with the cavity mode.

The difference between bistability with Rydberg transition [Eq. (3.10)] or with optical transitions [Eq. (3.11)] is best appreciated by using a simple graphical method, first introduced in [12] in the description of a Kerr medium. From the steady-state equation (3.10) follows

$$T_R(x) \equiv \frac{x}{y} = \frac{1}{1 + 2C\,\mathrm{sinc}^2(x/2)}, \tag{3.17}$$

so that the stationary states are given by the intersections of a transmission function $T_R(x)$, with a straight line x/y, whose slope is controlled by the input field amplitude y. Likewise, the steady-state equation for absorptive bistability in the optical regime (3.11) can be rewritten as

$$T_O(x) \equiv \frac{x}{y} = \frac{1}{1 + 2C_{\text{opt}}/(1 + x^2)}. \tag{3.18}$$

Both functions $T_R(x)$ and $T_O(x)$ vary between $1/(1+2C)$ and 1, which is a further justification for the definition (3.6) of the parameter C. In Fig. 2 the procedure described above is applied to the cases of optical and Rydberg transitions, with $C_{\text{opt}} = C = 10$. In the optical case [Fig. 2(a)] we find one or three stationary states, corresponding to monostability or bistability, respectively. With Rydberg atoms [Fig. 2(b)] we find one, three, or five stationary states, that is, multistability as a consequence of the oscillating nonlinearity. In this case, the oscillations are not produced by different cavity modes (only one mode is considered in our model), but by the Rabi cycles of the atoms in the cavity.

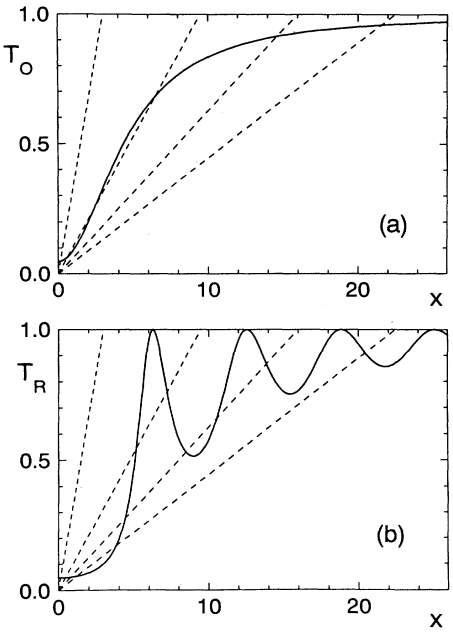

FIG. 2. Comparison between resonant stationary behavior for optical and Rydberg atomic transitions. The steady states are the intersections of a transmission curve $T(x)$ (solid line) with the line x/y (dashed lines), whose slope is governed by the input field y. (a) Optical transitions. Stationary states from Eq. (3.18) with $C_{\text{opt}} = 10$: bistability. (b) Rydberg transitions. Stationary states from Eq. (3.17) with $C = 10$: multistability.

Therefore the physical mechanism leading to bistability is quite different in each case. In absorptive bistability in optical systems, the physical origin of optical switching is the saturation of the atomic transition [4]. Actually, an experiment with a beam of Na atoms [13] has shown that the fluorescence intensity, proportional to the number of excited atoms, undergoes a hysteresis cycle (as a function of the incident power) similar to that of the transmitted power. In particular, with increasing input power, the field switches up when the atomic transition is saturated, while the population of the upper level switches up simultaneously due to the atomic bleaching. With decreasing input power, the internal field remains strong enough to keep the atoms close to saturation, until a lower input threshold is reached where the field switches down.

In Fig. 3 we show, for the case of Rydberg atoms, the calculated hysteresis cycles of the cavity field x [Fig. 3(a)] and of the atomic occupation probability of the upper level at the cavity exit $P_\uparrow(\tau)$ [Fig. 3(b)], versus the incident field amplitude y. Note that the quantity $P_\uparrow(\tau)$ [introduced in Eq. (3.3b)] is the dynamical variable of direct experimental relevance, because the count rate of atoms leaving the cavity in the upper level is the quantity actually monitored.

Let us consider the up-switching process in detail. Due to nonlinear absorption [$x \ll y$ in the lower branch of Fig. 3(a)], as y is increased from small values to $y \simeq y_\uparrow$, the excitation probability $P_\uparrow(\tau)$ [Fig. 3(b)] grows contin-

uously until the atomic population is almost completely inverted. Then, at $y = y_\uparrow$, the field switches up [Fig. 3(a)], while the excitation level jumps down [Fig. 3(b)], so that a drop in the upper-level count rate should be observed. A simple picture of this process can be given in terms of the atomic Bloch vector [Fig. 3(c)]. Initially ($y = 0$) the vector is pointing down. Then, with increasing y, it rotates continuously up to a nearly vertical position for $y = y_\uparrow$. On further increase of y, the vertical orientation becomes unstable and the Bloch vector discontinuously performs a rotation to an angle beyond 2π, where the system finds another stationary state, corresponding to more than one Bloch rotation during the time of flight through the cavity. With decreasing y, the Bloch vector rotates backwards and reaches the bleached state. At the down-switching threshold for the field, the population of the upper level switches up and the Bloch vector rotates discontinuously backwards to a new stable position. Unlike in the optical case, the hysteresis cycles of the cavity field and of the atomic population are manifestly different.

We conclude that bistability with Rydberg atoms is a novel effect, based on a physical mechanism quite different from standard absorptive optical bistability. In particular, the bleaching of the atomic medium is due to the motion of the Bloch vector (*Bloch switching*), which only

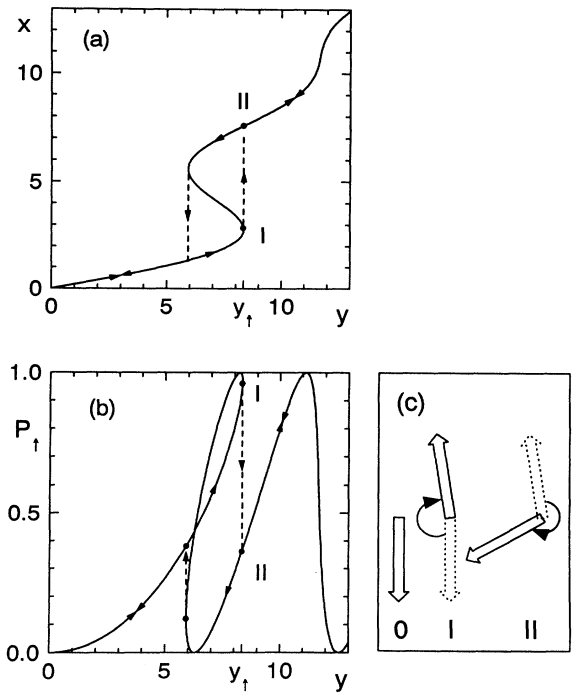

FIG. 3. Hysteresis cycle and the Bloch-switching mechanism from the resonant steady-state equation (3.10) with $C = 2$ for absorbing Rydberg atoms. (a) Cavity field amplitude x vs incident field amplitude y. (b) Occupation probability of the upper state at the cavity exit $P_\uparrow(\tau)$ vs incident field amplitude y. (c) Schematic representation of the evolution of the atomic Bloch vector in the up-switching process: the system, starting at $y = 0$ from state 0, jumps at $y = y_\uparrow$ from state I to state II.

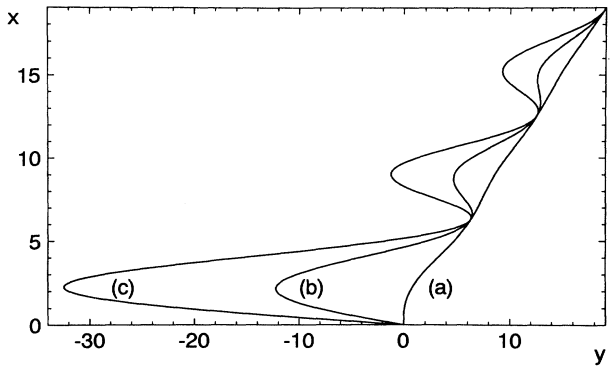

FIG. 4. Multistability in the nonlinear amplification with a beam of Rydberg atoms: cavity field amplitude x vs incident field amplitude y from the resonant steady-state equation (3.19). (a) $C = 0.5$; (b) $C = 5$; (c) $C = 12$.

for incident field amplitudes y well above the threshold $y_\uparrow$ approaches a regular rotatory behavior, corresponding to sinusoidal oscillations of $P_\uparrow(\tau)$ vs y. Saturation does not play any role here.

C. Nonlinear amplifier

In this section we briefly consider the amplifier regime in the resonant case, leaving a full discussion to a forthcoming paper [15]. The amplifier steady-state equation is

$$y = x - 4C\frac{1-\cos x}{x}. \tag{3.19}$$

Steady-state diagrams are shown in Fig. 4. Multistable behavior occurs like in the absorber case, and the *bleached states*, $x = y = 2m\pi$, are again present. The cooperative and asymptotic linear regimes are

$$y \ll 1: \quad x \simeq y/(1-2C), \tag{3.20}$$

$$y \gg 1, y \gg C: \quad x \simeq y. \tag{3.21}$$

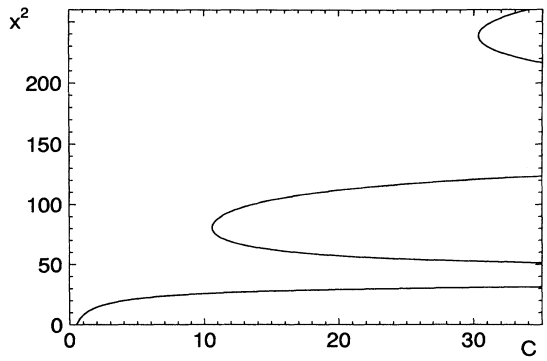

FIG. 5. Maser operation: dimensionless cavity field intensity x^2 vs cooperation parameter C, from the resonant steady-state equation (3.19) with incident field amplitude $y = 0$.

It must be kept in mind, however, that in the case of Eq. (3.19) not only the parts with negative slope are unstable, but also parts with $y < 0$, as can be easily obtained from the linear stability analysis described in Sec. IV.

As already observed, in the case $y = 0$ (no external field) the value $C = 1/2$ corresponds to the first micromaser threshold, when the trivial semiclassical no–masing state, $x = 0$, becomes unstable. For sufficiently high values of C, such as $C = 12$ in Fig. 4, further micromaser-type ($y = 0$) stable stationary states exist. The system successively reaches all of these states, when the control parameter y is used to cycle through the multiple loops, which implies passing $y = 0$ repeatedly. In the actual micromaser, these states are connected by fluctuations described by a full quantum treatment [7].

Let us now discuss the specific case of maser operation, $y = 0$, in our regime. The resonant steady-state equation can be written as $\mathrm{sinc}^2(x/2) = 1/2C$. The stationary states are the intersections of the curves $\mathrm{sinc}^2(x/2)$ with the horizontal line $1/2C$. Clearly, the number of these intersections increases with C ($C \geq 1/2$), which explains multistability. Figure 5 shows the scaled intensity x^2 vs C. Note the presence of two further branches of solutions for values of $C > 10.59$ and another pair for $C > 30.33$. In the limit of negligible fluctuations, the different branches are physically separated. As expected, by a different scaling we can reproduce the steady-state pump curve of a micromaser in the semiclassical limit [11]. This is demonstrated in Fig. 6, where we show $x^2/8C$ as a function of $\sqrt{2C}$. By the definitions (3.5) and (3.6), this corresponds to plotting n/N_{ex} versus a *pump parameter* $g\tau\sqrt{N_{\mathrm{ex}}}$, where n is the mean photon number and $N_{\mathrm{ex}} \equiv N/2k\tau$ is the average number of atoms passing through the resonator during one cavity field lifetime. This parametrization is suitable for the micromaser, where $k\tau \ll N \ll 1$, and in practice one describes the behavior of n vs $g\tau$ with $N_{\mathrm{ex}} \gg 1$ fixed [11]. On the other hand, when we plot x^2 vs C (Fig. 5) we really describe the behavior of n vs N_{ex}, where, in the spirit of the new regime considered, the average number of atoms in the cavity N can be varied as well as k or τ.

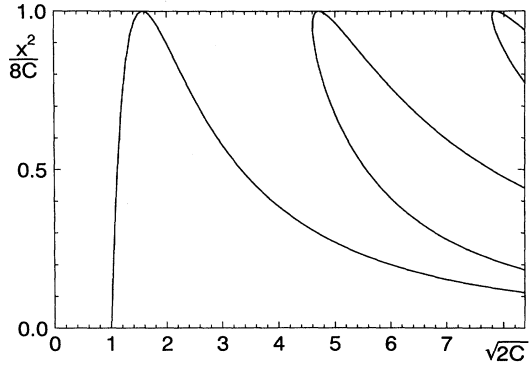

FIG. 6. Micromaser semiclassical dynamics recovered: scaled cavity field intensity $x^2/8C$ vs pump parameter $\sqrt{2C}$ from Eq. (3.19).

IV. LINEAR STABILITY ANALYSIS

In order to test the stability of the stationary states discussed in Sec. III, we consider the Maxwell-Bloch equations (2.1) on resonance ($\delta = \theta = 0$), and introduce the real and imaginary parts of the field and polarization variables, $\alpha_0(t)$ and $r^{\pm}(z',t)$, obtaining

$$\frac{d}{dt} \times \begin{Bmatrix} \mathrm{Re}[\alpha_0(t)] \\ \mathrm{Im}[\alpha_0(t)] \end{Bmatrix} = -k \times \begin{Bmatrix} \mathrm{Re}[\alpha_0(t)] - \alpha_{\mathrm{in}} \\ \mathrm{Im}[\alpha_0(t)] \end{Bmatrix} + \frac{gN}{\tau} \int_0^{\tau} dz' \begin{Bmatrix} \mathrm{Re}[r^{\pm}(z',t)] \\ \mathrm{Im}[r^{\pm}(z',t)] \end{Bmatrix}, \tag{4.1a}$$

$$\left(\frac{\partial}{\partial t} + \frac{\partial}{\partial z'}\right) \times \begin{Bmatrix} \mathrm{Re}[r^{\pm}(z',t)] \\ \mathrm{Im}[r^{\pm}(z',t)] \end{Bmatrix} = 2g\, r_3(z',t) \times \begin{Bmatrix} \mathrm{Re}[\alpha_0(t)] \\ \mathrm{Im}[\alpha_0(t)] \end{Bmatrix}, \tag{4.1b}$$

$$\left(\frac{\partial}{\partial t} + \frac{\partial}{\partial z'}\right) r_3(z',t) = -2g\{\mathrm{Re}[\alpha_0(t)]\mathrm{Re}[r^{\pm}(z',t)] + \mathrm{Im}[\alpha_0(t)]\mathrm{Im}[r^{\pm}(z',t)]\}. \tag{4.1c}$$

Next we set

$$\begin{Bmatrix} \mathrm{Re}[\alpha_0(t)] \\ \mathrm{Im}[\alpha_0(t)] \\ \mathrm{Re}[r^{\pm}(z',t)] \\ \mathrm{Im}[r^{\pm}(z',t)] \\ r_3(z',t) \end{Bmatrix} = \begin{Bmatrix} \mathrm{Re}(\alpha_0) & + & \mathrm{Re}[\delta\alpha_0(t)] \\ \mathrm{Im}(\alpha_0) & + & \mathrm{Im}[\delta\alpha_0(t)] \\ \mathrm{Re}[r^{\pm}(z')] & + & \mathrm{Re}[\delta r^{\pm}(z',t)] \\ \mathrm{Im}[r^{\pm}(z')] & + & \mathrm{Im}[\delta r^{\pm}(z',t)] \\ r_3(z') & + & \delta r_3(z',t) \end{Bmatrix}, \tag{4.2}$$

where on the right-hand side α_0, $r^{\pm}(z')$, and $r_3(z')$ denote the stationary values of these variables, and linearize Eqs. (4.1) around the steady state. By introducing the usual ansatz [14]

$$\begin{Bmatrix} \mathrm{Re}[\delta\alpha_0(t)] \\ \mathrm{Im}[\delta\alpha_0(t)] \\ \mathrm{Re}[\delta r^{\pm}(z',t)] \\ \mathrm{Im}[\delta r^{\pm}(z',t)] \\ \delta r_3(z',t) \end{Bmatrix} = e^{\lambda t} \times \begin{Bmatrix} \mathrm{Re}(\delta\alpha_0) \\ \mathrm{Im}(\delta\alpha_0) \\ \mathrm{Re}[\delta r^{\pm}(z')] \\ \mathrm{Im}[\delta r^{\pm}(z')] \\ \delta r_3(z') \end{Bmatrix} + \mathrm{c.c.}, \tag{4.3}$$

where λ is the eigenvalue of the linearized problem, we obtain the equations

$$(\lambda + k) \times \left\{ \begin{array}{c} \mathrm{Re}(\delta\alpha_0) \\ \mathrm{Im}(\delta\alpha_0) \end{array} \right\} - \frac{gN}{\tau} \int_0^\tau dz' \left\{ \begin{array}{c} \mathrm{Re}[\delta r^{\pm}(z')] \\ \mathrm{Im}[\delta r^{\pm}(z')] \end{array} \right\} = 0, \tag{4.4a}$$

$$\left(\lambda + \frac{d}{dz'}\right) \times \left\{ \begin{array}{c} \mathrm{Re}[\delta r^{\pm}(z')] \\ \mathrm{Im}[\delta r^{\pm}(z')] \end{array} \right\} - 2g \left[\delta r_3(z') \times \left\{ \begin{array}{c} \mathrm{Re}(\alpha_0) \\ \mathrm{Im}(\alpha_0) \end{array} \right\} + r_3(z') \times \left\{ \begin{array}{c} \mathrm{Re}(\delta\alpha_0) \\ \mathrm{Im}(\delta\alpha_0) \end{array} \right\} \right] = 0, \tag{4.4b}$$

$$\left(\lambda + \frac{d}{dz'}\right) \delta r_3(z') + 2g\{\mathrm{Re}(\alpha_0)\mathrm{Re}[\delta r^{\pm}(z')] + \mathrm{Im}(\alpha_0)\mathrm{Im}[\delta r^{\pm}(z')] + \mathrm{Re}(\delta\alpha_0)\mathrm{Re}[r^{\pm}(z')] + \mathrm{Im}(\delta\alpha_0)\mathrm{Im}[r^{\pm}(z')]\} = 0. \tag{4.4c}$$

According to the ansatz (4.3), a stationary state is stable if, and only if, $\mathrm{Re}(\lambda) < 0$ for all eigenvalues λ which satisfy the characteristic equations derived subsequently.

First, we consider the linearized Bloch equations (4.4b) and (4.4c). By a simple but lengthy calculation using Eqs. (3.3), we obtain a closed third-order differential equation for the deviation $\delta r_3(z')$ (the prime denoting d/dz')

$$\delta r_3''' + 3\lambda \delta r_3'' + \left(\Omega_0^2 + 3\lambda^2\right) \delta r_3' + \lambda \left(\Omega_0^2 + \lambda^2\right) \delta r_3 = -\frac{\Omega_0}{2} \frac{\mathrm{Re}(\delta\alpha_0)}{\alpha_0} \left[\left(2\Omega_0^2 - \lambda^2\right) \sin(\Omega_0 z') - 3\lambda\Omega_0 \cos(\Omega_0 z') \right]. \tag{4.5}$$

The initial conditions $\delta r^{\pm}(0) = \delta r_3(0) = 0$, together with Eqs. (4.4b) and (4.4c), imply that $\delta r_3(0) = \delta r_3'(0) = 0$ and $\delta r_3''(0) = {\Omega_0}^2 \mathrm{Re}(\delta\alpha_0/\alpha_0)$. Hence the solution of Eq. (4.5) is

$$\delta r_3(z') = \frac{\Omega_0}{2} \frac{1 - e^{-\lambda z'}}{\lambda} \frac{\mathrm{Re}(\delta\alpha_0)}{\alpha_0} \sin(\Omega_0 z'). \tag{4.6}$$

The result (4.6) is inserted into Eqs. (4.4b), whose solutions are

$$\begin{aligned} \mathrm{Re}[\delta r^{\pm}(z')] &= -\frac{\Omega_0}{2} \frac{1 - e^{-\lambda z'}}{\lambda} \frac{\mathrm{Re}(\delta\alpha_0)}{\alpha_0} \cos(\Omega_0 z'), \\ \mathrm{Im}[\delta r^{\pm}(z')] &= -\frac{\Omega_0}{2} \frac{1}{\Omega_0^2 + \lambda^2} \frac{\mathrm{Im}(\delta\alpha_0)}{\alpha_0} \left\{ \Omega_0 \sin(\Omega_0 z') + \lambda \left[\cos(\Omega_0 z') - e^{-\lambda z'} \right] \right\}. \end{aligned} \tag{4.7}$$

Expressions (4.7) provide the source terms in the linearized equations (4.4a) for the real and imaginary parts of the field deviations, $\mathrm{Re}(\delta\alpha_0)$ and $\mathrm{Im}(\delta\alpha_0)$. From Eqs. (4.7), using the definitions (3.5) and (3.6) of x and C, we obtain the following eigenvalue equations:

$$(\lambda + k) \times \left\{ \begin{array}{c} \mathrm{Re}(\delta x) \\ \mathrm{Im}(\delta x) \end{array} \right\} = \frac{4Ck}{x^2 + \lambda^2\tau^2} \left\{ \begin{array}{c} J_1(x;\lambda\tau)\mathrm{Re}(\delta x) \\ J_2(x;\lambda\tau)\mathrm{Im}(\delta x) \end{array} \right\}, \tag{4.8}$$

where

$$\begin{aligned} J_1(x;\lambda\tau) &= 1 - e^{-\lambda\tau}\cos x - \frac{1}{\lambda\tau}\left(1 - e^{-\lambda\tau} + \frac{\lambda^2\tau^2}{x^2}\right) x \sin x, \\ J_2(x;\lambda\tau) &= \cos x - e^{-\lambda\tau} - \lambda\tau\,\mathrm{sinc}\, x. \end{aligned} \tag{4.9}$$

Finally, from Eqs. (4.8) we obtain the characteristic equations

$$\lambda + k - \frac{4Ck}{x^2 + \lambda^2\tau^2} \left\{ \begin{array}{c} J_1(x;\lambda\tau) \\ J_2(x;\lambda\tau) \end{array} \right\} = 0. \tag{4.10}$$

Instead of solving Eqs. (4.10) for λ directly, we will calculate the stability boundary of the stationary solutions in the space of the system parameters C, k, τ, and y. Instead of the input field y, we will use the stationary value x of the intracavity field, which is linked to y by the steady-state equation (3.10). One part of the boundary is characterized by the fact that the sign of a real eigenvalue λ changes sign, i.e., $\lambda = 0$. For $\lambda = 0$, Eqs. (4.10) reduce to

$$1 - 4C\left(\frac{1 - \cos x}{x^2} - \mathrm{sinc}\, x\right) = \frac{dy}{dx} = 0, \tag{4.11a}$$

$$1 + 4C\frac{1 - \cos x}{x^2} = \frac{y}{x} = 0, \tag{4.11b}$$

where we have used the steady-state equation (3.10). Equation (4.11a) defines the turning points of the steady-state curve and confirms that in the steady-state $x(y)$ diagrams all branches with negative slope are unstable. On the other hand, Eq. (4.11b) is never satisfied. [Only in the amplifier case it can be satisfied, indicating the instability of the steady-state curve sections with $y < 0$ (see, e.g., Fig. 4).]

The remaining part of the instability boundary is characterized by the fact that the real part of a pair of complex conjugate eigenvalues changes sign, i.e.,

$$\lambda = i\nu, \quad \nu \text{ real}, \quad \nu \neq 0. \tag{4.12}$$

When this part of the boundary is crossed, the stationary state of the system disappears and a new state appears, displaying oscillations of frequency ν (Hopf bifurcation).

By introducing the dimensionless quantity

$$\bar{\nu} \equiv \nu\tau, \tag{4.13}$$

substituting Eqs. (4.12) and (4.13) into the first of Eqs. (4.10), and splitting into real and imaginary parts, we obtain the two equations

$$1 = \frac{4C}{x^2 - \bar{\nu}^2}\left(1 - \cos x \cos\bar{\nu} - x \sin x \,\mathrm{sinc}\,\bar{\nu}\right), \tag{4.14a}$$

$$\frac{\bar{\nu}}{k\tau} = \frac{4C}{x^2 - \bar{\nu}^2}\left[\cos x \sin\bar{\nu} + \frac{1}{\bar{\nu}}\left(1 - \cos\bar{\nu} - \frac{\bar{\nu}^2}{x^2}\right) x \sin x\right]. \tag{4.14b}$$

Eliminating $\bar{\nu}$ from Eqs. (4.14) results in an equation in parameter space, which defines another part of the stability boundary. On the other hand, by applying the same procedure to the second of Eqs. (4.10) we obtain the two equations

$$1 = -\frac{4C}{x^2 - \bar{\nu}^2}\left(\cos\bar{\nu} - \cos x\right), \tag{4.15a}$$

$$\frac{\bar{\nu}}{k\tau} = -\frac{4C}{x^2 - \bar{\nu}^2}\left(\mathrm{sinc}\, x - \mathrm{sinc}\,\bar{\nu}\right), \tag{4.15b}$$

which, after elimination of $\bar{\nu}$, provide the last part of the boundary.

Equations (4.14) and (4.15) have been investigated numerically. They depend on the two parameters C and $k\tau$. It turns out that Eqs. (4.15a) and (4.15b) are never simultaneously satisfied. On the other hand, Eqs. (4.14a) and (4.14b) can hold simultaneously, provided that C is large enough ($C \geq 3.33$), i.e., has a value beyond the tristability threshold (see Table I), and provided that $k\tau$ is not too small.

In our numerical search for the solutions to Eqs. (4.14) we proceed as follows. For given values of C and $k\tau$, we look for a point x in the middle of one of the positive-slope parts of the steady-state curve, such that Eq. (4.14a) as well as Eq. (4.14b) has at least one solution for $\bar{\nu}$. If no such point exists, the values chosen for C or $k\tau$ are too small. When a suitable x has been found, we keep C and $k\tau$ fixed and vary x, until we reach a point for which Eqs. (4.14a) and (4.14b) have the same solution $\bar{\nu}$. Then, by construction, the values of C, x, and $k\tau$ define a point of the stability boundary, at which the system should display the onset of spontaneous oscillations of frequency $\bar{\nu}/\tau$. Two such points determine an unstable segment of the steady-state curve. Figure 7, where $C = 5$ and $k\tau = 3$, shows an example of instability occurring in the positive-slope part of the stationary $x(y)$ curve. The existence of such unstable domains crucially depends not only on C, but also on the product $k\tau$. For decreasing C or $k\tau$ these regions shrink and finally disappear.

This result of the analysis implies another remarkable difference from the optical case. As a matter of fact, in standard absorptive optical bistability there is no oscillatory instability [4]. Such instabilities may occur only in dispersive optical bistability, as predicted in [16] and experimentally observed in [17]. With Rydberg atoms, however, for high enough values of C, one should observe

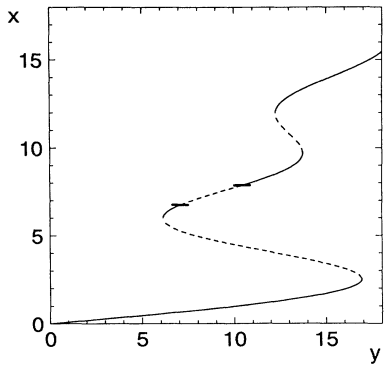

FIG. 7. Instability in the multistable absorption with a beam of Rydberg atoms. The dashed parts of the stationary diagram of cavity field amplitude x vs injected field amplitude y are unstable. The instability boundaries are calculated from Eqs. (4.14) with $C = 5$ and $k\tau = 3$. The unstable part of the stationary curve x(y) with *positive* slope extends from $x = 6.75$ ($\bar{\nu} = 3.06$) to $x = 7.88$ ($\bar{\nu} = 3.89$).

either multistability or instability, simply by changing the value of $k\tau$.

We leave to future work [15] the task of solving numerically the full nonlinear equations (3.1) in the unstable parameter domain, where we expect the system to approach a state in which the output intensity exhibits undamped oscillations.

V. INHOMOGENEOUS EFFECTS

The analysis presented so far was based on the idealizing assumption that all atoms have the same velocity and the same transition frequency. In an actual experiment, however, the atomic beam can only be prepared with a finite velocity spread. Furthermore, the atomic levels are subject to random Stark shifts due to stray electric fields. We have investigated how the behavior of the nonlinear absorber is modified by these effects.

We start by observing that the dynamics of all atoms with a given velocity v is determined by Eqs. (2.1b) and (2.1c), independent of the presence of other atoms with different velocities. The reason is that atoms do not interact with each other directly, but only via the cavity field α. If, for the moment, we restrict ourselves to the resonant case $\theta = \delta = 0$, the stationary solution for the r^- component corresponding to the subgroup of atoms with velocity v is

$$r_v^-(z) = \frac{1}{2}\sin\left(\Omega_0 \frac{z}{v}\right). \tag{5.1}$$

Radiation from all atoms contributes to the cavity field α_0. Accordingly, the atomic source term in Eq. (3.1a) has to be integrated over velocity, weighted by a distribution function $P(v)$,

$$\alpha_{\mathrm{in}} = \alpha_0 + \frac{g^2 N \alpha_0}{k\Omega_0^2 L}\int_0^\infty dv\, P(v) v \left(1 - \cos\frac{\Omega_0 L}{v}\right). \tag{5.2}$$

We have examined two cases of particular practical interest: a Maxwellian velocity distribution and a Gaussian velocity profile.

A. Thermal velocity distribution

The velocity distribution of a thermal beam of atoms, originating from an effusive source and excited to a Rydberg level, is described by a Maxwellian function

$$P(v) = \frac{4}{\sqrt{\pi}\beta^3} v^2 e^{-(v/\beta)^2}. \tag{5.3}$$

The parameter β is the most probable velocity in the beam. Inserting Eq. (5.3) into Eq. (5.2), the steady-state equation for the field now reads

$$\alpha_{\rm in} = \alpha_0 + \frac{4g^2 N \alpha_0 \beta}{\sqrt{\pi} k \Omega_0^2 L}\left[\frac{1}{2} - I(\Omega_0 L/\beta)\right], \tag{5.4}$$

with I being the first Ramsey integral [18]

$$I(x) = \int_0^\infty dw\, w^3 e^{-w^2} \cos\frac{x}{w}. \tag{5.5}$$

Analogous to Eq. (3.5) we can transform to scaled variables x and y

$$x = 2g\alpha_0 L/\beta, \qquad y = 2g\alpha_{\rm in} L/\beta. \tag{5.6}$$

Using (5.6) we obtain the scaled steady-state equation for a thermal beam of Rydberg atoms

$$y = x\left[1 + 4C\,\frac{1 - 2I(x)}{x^2}\right]. \tag{5.7}$$

The cooperation parameter C is defined as in Eq. (3.6) with τ replaced by $\bar{\tau} = 2L/\sqrt{\pi}\beta$, which denotes the average transit time of the atoms through the resonator.

In the asymptotic limit $y \ll 1$, Eq. (5.7) approaches the low field behavior of Eqs. (3.10) and (3.11)

$$x \simeq \frac{y}{1 + 2C}. \tag{5.8}$$

Results for the steady-state equation (5.7) are shown in Fig. 8 for different values of the parameter C. There is bistable behavior, if C is larger than the threshold value

$$C_{\rm thr} = 2.300. \tag{5.9}$$

Multistability, as found in the monoenergetic case, is absent, even for arbitrarily high values of C. This can be understood by looking at the properties of the function $I(x)$. For $x \ll 2\pi$, $2I(x)$ behaves like the cosine function. Consequently, the first hysteresis loop in the steady-state solution for the cavity field x shows the same behavior as in the monoenergetic case. For larger values of x, $I(x)$ approaches a constant value of 0. This corresponds to the washing out of Rabi oscillations by averaging over a broad velocity distribution.

The hysteresis loop for the cavity field in the case of a

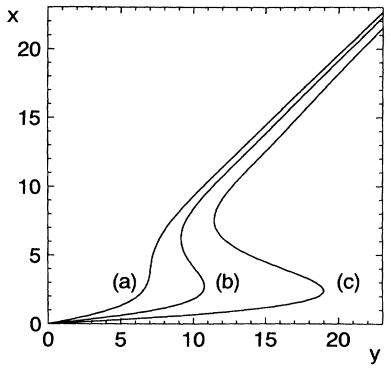

FIG. 8. Multistability for a thermal beam of Rydberg atoms: cavity field amplitude x vs incident field amplitude y from the resonant steady-state equation (5.7). (a) $C = 2$; (b) $C = 4$; (c) $C = 8$.

Maxwellian velocity distribution looks similar to the result obtained in the standard case of absorptive optical bistability with radiative broadening. This might suggest that the distribution of transit times in a Rydberg-atom experiment has the same effect as spontaneous decay for optical transitions. That is, however, not the case. The mechanism leading to bistability with Rydberg atoms is distinct from saturated absorption, even if the Rabi oscillations are washed out. This is apparent in the behavior of the upper-level population $P_\uparrow(z = L)$ of the atoms leaving the cavity, that was defined in Eq. (3.3b). Averaging over velocity one obtains

$$\begin{aligned} P_\uparrow(z = L) &= \frac{1}{2} + \int_0^\infty dv\, P(v) r_3(z = L)_v \\ &= \frac{1}{2} - \frac{2}{\sqrt{\pi}} I_2(x), \end{aligned} \tag{5.10}$$

where the function I_2 is defined as

$$I_2 = \int_0^\infty dw\, w^2 e^{-w^2} \cos\frac{x}{w}. \tag{5.11}$$

Plotting $P_\uparrow(L)$ as a function of the scaled input field y in Fig. 9, we see that the hysteresis cycle still has the char-

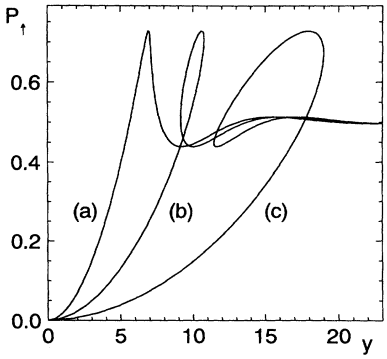

FIG. 9. Hysteresis cycle in the upper level occupation probability $P_\uparrow$ at the cavity exit as a function of the incident field amplitude y. The parameters correspond to those of Fig. 8. (a) $C = 2$; (b) $C = 4$; (c) $C = 8$.

acteristic butterfly shape that was found in the monoenergetic case. This is in contrast to the simple ring-shaped hysteresis loop followed by the population variable in the standard theory of optical bistability.

B. Gaussian velocity distribution

While a beam with a Maxwellian velocity distribution displays bistable behavior at most, the question arises if multiple stable states can be observed by narrowing the velocity distribution, for example, by applying velocity selection.

We have investigated the case of a Gaussian velocity profile with an average velocity v_0 and a relative velocity spread σ,

$$P(v) = \frac{1}{\sigma v_0 \sqrt{\pi}} e^{-(v/v_0 - 1)^2/\sigma^2}. \tag{5.12}$$

Inserting Eq. (5.12) into (5.2) and transforming to the scaled variables (3.5) we obtain

$$y = x\left[1 + 4C\,\frac{1 - G_\sigma(x)}{x^2}\right], \tag{5.13}$$

where we have introduced the function

$$G_\sigma(x) = \frac{1}{\sigma\sqrt{\pi}} \int_{-\infty}^{\infty} dw\; w e^{-\left(\frac{w-1}{\sigma}\right)^2} \cos\frac{x}{w}. \tag{5.14}$$

The cooperation parameter C again is given by Eq. (3.6), with τ replaced by $\tau_0 = L/v_0$. In the limit $\sigma \to 0$, $G_\sigma(x)$ approaches $\cos(x)$ and Eq. (5.13) coincides with the monoenergetic equation (3.10).

As shown in Fig. 10, the steady-state equation (5.13) features multistable solutions. The corresponding threshold values $C_{\rm thr}$ now depend on the velocity spread σ. The C values necessary to obtain a given order of multistability increase with σ. It is interesting to note that multistability can be found even when σ is comparable to the width of the thermal velocity distribution (5.3). Obviously not only the width, but also the shape of $P(v)$ is important.

C. Inhomogeneous Stark broadening

In Rydberg-atom experiments, transit time is not the only source of broadening. Due to the large polarizability of highly excited states, stray electric fields lead to a noticeable random shift of the transition frequency between adjacent Rydberg levels.

The method for taking into account Stark broadening is analogous to that employed for velocity effects. For the sake of simplicity we make the assumption that the frequency shift for a given atom does not change during the interaction with the cavity field, i.e., the detuning is not a function of z. We assume a monoenergetic beam at first. In that case all atoms with detuning δ are described by the steady-state solution (3.3).

We model the inhomogeneous line shape by a Gaussian

$$\Pi(\delta) = \frac{\tau}{\Gamma\sqrt{\pi}} e^{-(\delta\tau/\Gamma)^2}. \tag{5.15}$$

Γ is the dimensionless inhomogeneous linewidth, defined in units of the inverse transit time τ^{-1}, which plays the role of a homogeneous linewidth, here.

All atoms contribute to the cavity field α_0. Therefore the atomic source term in the field equation (3.1a) must be integrated over detuning, weighted by the line shape $\Pi(\delta)$. Taking advantage of the symmetry of $\Pi(\delta)$ and transforming to scaled variables, we arrive at a steady-state equation for the field

$$y = x\,[1 + 4C\,J_\Gamma(x)]\,, \tag{5.16}$$

using the parameter C as defined in Eq. (3.6). The integral in Eq. (5.16) is

$$J_\Gamma(x) = \frac{2}{\Gamma\sqrt{\pi}} \int_0^\infty ds\; e^{-(s/\Gamma)^2} \frac{1 - \cos\sqrt{x^2 + s^2}}{x^2 + s^2}. \tag{5.17}$$

The resulting steady-state curves are shown in Fig. 11. As long as the condition $\Gamma < 1$ is fulfilled, i.e., transit broadening prevails, the steady state is not much differ-

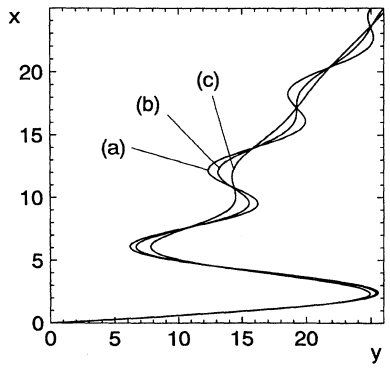

FIG. 10. Multistability for a beam of Rydberg atoms with a Gaussian velocity distribution: cavity field amplitude x vs incident field amplitude y from the steady-state equation (5.13) for $C = 8$. (a) $\sigma = 0$; (b) $\sigma = 0.1$; (c) $\sigma = 0.2$.

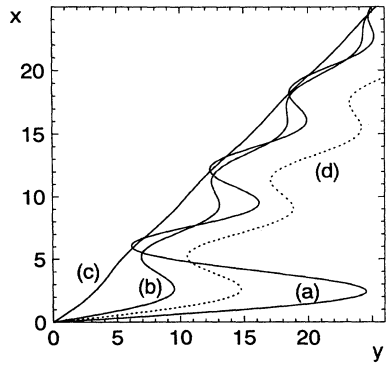

FIG. 11. Multistability for a monoenergetic beam of Stark-broadened Rydberg atoms: cavity field amplitude x vs incident field amplitude y from the steady-state equation (5.16) for $C = 8$. (a) $\Gamma = 1$; (b) $\Gamma = 10$; (c) $\Gamma = 100$. For comparison (d) shows the hysteresis for $\Gamma = 100$ and $C = 120$.

ent from the homogeneous broadening case discussed in Sec. III B. If, on the other hand, $\Gamma \gg 1$, the nonlinear part of the steady-state equation (5.16) is strongly suppressed. In contrast to the case of a thermal velocity distribution, however, $J_\Gamma(x)$ displays multiple oscillations, even for arbitrarily large Γ. Therefore, the multistable regime can be reached by increasing the parameter C sufficiently, even if in homogeneous broadening dominates (cf. the dotted curve in Fig. 11).

D. Inhomogeneous broadening in a thermal beam

A realistic model for a Rydberg-atom experiment has to take into account both velocity and Stark broadening effects. Therefore we finally combine the results of the previous sections to obtain a general solution for a beam of atoms with a thermal velocity and a Gaussian frequency distribution. Proceeding as before, we obtain the following steady-state equation:

$$y = x\,[1 + 4C\,K_\Gamma(x)]\,, \tag{5.18}$$

with C, x, and y defined as in Sec. V A. In this case, $K_\Gamma(x)$ contains a double integral, one over the velocity distribution and one over the frequency distribution. One of the integrals, however, can be evaluated analytically, and $K_\Gamma(x)$ finally takes the form

$$K_\Gamma(x) = \frac{1}{\Gamma^2}\int_0^\infty dw\,\frac{w^3}{\sqrt{1+w^2}}\,e^{-(wx/\Gamma)^2}\left[2\left(\frac{x}{\Gamma}\right)^2 + \frac{1}{1+w^2}\right]\left[1-\cos\frac{\Gamma}{w}\right]. \tag{5.19}$$

We have calculated the steady-state equation for $C = 8$ for three different values of the inhomogeneous linewidth Γ (Fig. 12). As expected for a thermal velocity distribution, no multistability is found. Above the bistability threshold, the size of the hysteresis loop for a given C is governed by the parameter Γ. The dotted curve (d) in Fig. 12 demonstrates that by increasing C for fixed Γ the bistability region can be reached. At $\Gamma = 10$ and $C = 23$, for example, there is again a pronounced hysteresis.

Equations (5.18) and (5.19) are our final result for the theory of resonant bistability in a Rydberg-atom system. They may be used to estimate the parameters necessary for the observation of bistability in such a system and to predict the size of the effect.

VI. EXPERIMENTAL FEASIBILITY

We briefly consider if the effects predicted in this paper are within experimental reach. We choose parameters corresponding to conditions in a Rydberg-atom experiment being set up in Munich at the Max-Planck-Institut für Quantenoptik. As in the micromaser, transitions between levels of ^{85}Rb are used. The atomic beam has a thermal velocity distribution with an average time of flight through the resonator $\bar{\tau} \approx 100\ \mu$s. Atom-field coupling constants g for Rb Rydberg states are typically larger than $10^3\ \mathrm{s}^{-1}$. Transition frequencies at a principal quantum number $n \approx 50$ are around $160 \times 10^9\ \mathrm{s}^{-1}$. A quality factor $Q = 10^8$ of a superconducting resonator can be realized with a ^{4}He cryostat. Using Eq. (2.2), we obtain a field decay time k of about $800\ \mathrm{s}^{-1}$. Inserting these values in Eq. (3.6) for the cooperation parameter, we have

$$C = \frac{Ng^2\bar{\tau}}{4k} \geq 0.03N. \tag{6.1}$$

The bistability threshold for a thermal beam (5.9) is reached for $N = 74$ atoms in the cavity, a value in agreement with our assumption of a mesoscopic system. As no velocity selection is provided, higher-order multistability cannot be observed.

There are two feasible modifications of this experimental setup. First, the quality factor of the cavity may be increased to a value of $Q \approx 10^{10}$, as was achieved in the micromaser experiment [6]. Under these conditions $C \approx 3N$ and an average number of $N = 0.74$ atoms in the cavity is sufficient to observe the onset of bistability. Increasing the Q factor obviously takes the system from the mesoscopic to the microscopic regime $N < 1$. Another feature of such a system is that the required atomic flux $N/\bar{\tau}$ of only $7000\ \mathrm{s}^{-1}$ can be realized even when a 5% velocity selection is applied to the beam. In that case, the results of Sec. V B imply the appearance of multistability.

The setup described above may be modified in yet another way. It is possible to use a Rydberg transition with a very high value of the coupling constant, $g \approx 10^5\ \mathrm{s}^{-1}$. In this case, even a quality factor as low as $Q \approx 10^6$ is sufficient to obtain the same cooperation parameter $C \approx 3N$ as above. For such a moderate Q value, the

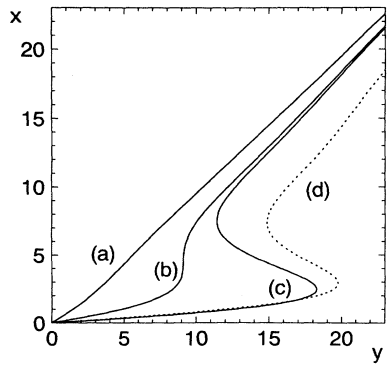

FIG. 12. Multistability with a thermal beam of Stark-broadened Rydberg atoms: cavity field amplitude x vs. incident field amplitude y from the steady-state equation (5.18) for $C = 8$. (a) $\Gamma = 1$; (b) $\Gamma = 10$; (c) $\Gamma = 100$. For comparison (d) shows the hysteresis for $\Gamma = 10$ and $C = 23$.

product $k\tau$ has a value around 8, i.e., the system is in the region where instabilities should appear in the positive-slope branches of the steady-state curve.

It is interesting to note that for a coupling constant g as large as $10^5\ s^{-1}$, the product $2g\tau$, which appears in the scaling (3.5) for the field variables, is on the order of 20. Consequently, a single photon is a sufficient field to cycle the system through the hysteresis loop. In this regime, the mesoscopic treatment given in this paper is no longer valid because quantum and thermal fluctuations can no longer be ignored. Nevertheless experiments in such a parameter range might serve as a test, if the semiclassical treatment is still a valid description of the average behavior of the system.

VII. CONCLUSION

Summing up, we have investigated the mechanism leading to multistability in a system of two-level Rydberg atoms interacting with a single resonant mode of a microwave cavity. The effect is based on the Rabi oscillations of the atoms during their time of flight through the cavity and the absence of damping by spontaneous emission. From a Bloch equation model we have derived an analytic steady-state equation and calculated multistability thresholds.

The quantity actually monitored in a Rydberg-atom experiment is the level population. Therefore we have also determined the steady-state hysteresis curves for the upper-level population. It has a characteristic butterfly shape, distinct from the standard case of bistability based on saturated absorption. Another feature not present in the standard theory for the resonant case is that the system may develop domains of instability, even in positive-slope regions of the steady-state curve.

In order to match our theory as closely as possible to experimental conditions, we have investigated the influence of a velocity distribution of the atoms and of Stark broadening in stray electric fields. We have found that a Gaussian velocity distribution increases the multistability thresholds, while with a thermal atomic beam, only bistability can be achieved. Adding inhomogeneous line broadening does not alter the general picture, but leads to a further increase of the thresholds for multistability.

A comparison with parameters achieved in present Rydberg-atom experiments shows that multistable behavior, as well as instabilities in the upper branches of the hysteresis curve are well within experimental reach. It even seems feasible to investigate the system in a regime beyond the analysis presented here, where quantum fluctuations of the cavity field become important.

ACKNOWLEDGMENTS

We acknowledge helpful discussions with Marlan O. Scully and Ennio Arimondo. This work was partially supported by CNR Grant No. 92.01369.ct02.

[1] E. T. Jaynes and F. W. Cummings, Proc. IEEE **51**, 89 (1963).

[2] H. Haken, *Laser Theory*, edited by S. Flügge, Handbuch der Physik Vol. XXV/2c (Springer, Berlin, 1970); M. Sargent III, M. O. Scully, and W. E. Lamb, *Laser Physics* (Addison-Wesley, Reading, MA, 1974).

[3] R. H. Dicke, Phys. Rev. **93**, 99 (1954); N. E. Rehler and J. H. Eberly, Phys. Rev. A **3**, 1735 (1973); R. Bonifacio, R. Schwendimann, and F. Haake, *ibid.* **4**, 382 (1971); **4**, 854 (1971); R. Bonifacio and L. A. Lugiato, *ibid.* **11**, 1507 (1975); **12**, 587 (1975).

[4] L. A. Lugiato, in *Progress in Optics*, edited by E. Wolf (North-Holland, Amsterdam, 1984), Vol. XXI, p. 69 ff.; H. M. Gibbs, *Optical Bistability: Controlling Light by Light* (Academic, New York, 1985).

[5] See, e.g., S. Haroche, in *New Trends in Atomic Physics*, edited by G. Grynberg and R. Stora (North-Holland, Amsterdam, 1984); H. J. Carmichael, R. J. Brecha, M. G. Raizen, H. J. Kimble, and P. R. Rice, Phys. Rev. A **40**, 5516 (1989); P. Meystre, in *Progress in Optics*, edited by E. Wolf (North-Holland, Amsterdam, 1992); Vol. 30; S. Haroche and D. Kleppner, Phys. Today **42** (1), 24 (1989).

[6] D. Meschede, H. Walther, and G. Müller, Phys. Rev. Lett. **54**, 551 (1985); G. Rempe, F. Schmidt-Kaler, and H. Walther, *ibid.* **64**, 2783 (1990); G. Rempe and H. Walther, Phys. Rev. A **42**, 1650 (1990).

[7] Micromaser theories have been developed in P. Filipowicz, J. Javanainen, and P. Meystre, Phys. Rev. A **34**, 3077 (1986); L. A. Lugiato, M. O. Scully, and H. Walther, *ibid.* **36**, 740 (1987).

[8] A two-photon micromaser has been realized by M. Brune, J. M. Raimond, P. Goy, L. Davidovitch, and S. Haroche, Phys. Rev. Lett. **59**, 1899 (1987).

[9] G. Rempe, R. J. Thompson, R. J. Brecha, W. D. Lee, and H. J. Kimble, Phys. Rev. Lett. **67**, 1727 (1991).

[10] A. N. Oraevski, T. V. Sarkisyan, D. J. Jones, and D. K. Bandy, Sov. J. Quantum Electron. **22**, 213 (1992).

[11] A. M. Guzman, P. Meystre, and E. M. Wright, Phys. Rev. A **40**, 2471 (1989).

[12] F. S. Felber and J. H. Marburger, Appl. Phys. Lett. **28**, 731 (1976).

[13] D. E. Grant and H. J. Kimble, Opt. Commun. **44**, 415 (1983).

[14] See, e.g., L. M. Narducci and N. B. Abraham, *Laser Physics and Laser Instabilities* (World Scientific, Singapore, 1988); L. A. Lugiato and L. M. Narducci, Phys. Rev. A **32**, 1567 (1985); L. A. Lugiato, L. M. Narducci, and M. F. Squicciarini, *ibid.* **34**, 3101 (1986).

[15] F. Casagrande, L. A. Lugiato, W. Lange, and H. Walther (unpublished).

[16] L. A. Lugiato, L. M. Narducci, D. K. Bandy, and C. A. Pennise, Opt. Commun. **43**, 281 (1982).

[17] L. A. Orozco, A. T. Rosenberger, and H. J. Kimble, Phys. Rev. Lett. **53**, 2547 (1984).

[18] N. F. Ramsey, *Molecular Beams* (Oxford University Press, Oxford, 1956).